Kilohertz Rotation of Nanorods Propelled by Ultrasound, Traced by Microvortex Advection of Nanoparticles

Andrew L. Balk,[†,‡,△] Lamar O. Mair, [†,‡,△,▽] Pramod P. Mathai, [†,§] Paul N. Patrone, [†,‖,⊥] Wei Wang,[#,□] Suzanne Ahmed,[#] Thomas E. Mallouk,[#] J. Alexander Liddle,[†] and Samuel M. Stavis[†,*]

[†]Center for Nanoscale Science and Technology, National Institute of Standards and Technology, Gaithersburg, Maryland 20899, United States, [‡]Maryland Nanocenter, University of Maryland, College Park, Maryland 20742, United States, [§]Department of Materials Science and Engineering, University of Maryland, College Park, Maryland 20742, United States, [‖]Institute for Research in Electronics and Applied Physics, University of Maryland, College Park, Maryland 20742, United States, [⊥]Institute for Mathematics and its Applications, University of Minnesota, Minneapolis, Minnesota 55455, United States, and [#]Department of Chemistry, The Pennsylvania State University, University Park, Pennsylvania 16802, United States. [△]A. L. Balk and L. O. Mair contributed equally to this research. [▽]Present address: Weinberg Medical Physics LLC, Bethesda, Maryland 20817, United States. [□]Present address: School of Material Science and Engineering, Shenzhen Graduate School, Harbin Institute of Technology, University Town, Shenzhen 518055, China. *Address correspondence to samuel.stavis@nist.gov.

ABSTRACT. We measure the microvortical flows around gold nanorods propelled by ultrasound in water using polystyrene nanoparticle as optical tracers. We infer the rotational frequencies of such nanomotors assuming a hydrodynamic model of this interaction. In this way, we find that nanomotors rotate around their longitudinal axes at frequencies of up to ≈ 2.5 kHz, or $\approx 150,000$ RPM, in the planar pressure node of a half–wavelength layered acoustic resonator driven at ≈ 3 MHz with an acoustic energy density of $< 10 \text{ J} \cdot \text{m}^{-3}$. The corresponding tangential speeds of up to $\approx 2.5 \text{ mm} \cdot \text{s}^{-1}$ at a nanomotor radius of ≈ 160 nm are two orders of magnitude faster than the translational speeds of up to $\approx 20 \text{ μm} \cdot \text{s}^{-1}$. We also find that rotation and translation are independent modes of motion within experimental uncertainty. Our study is an important step towards understanding the behavior and fulfilling the potential of this dynamic nanotechnology for hydrodynamically interacting with biological media, as well as other applications involving nanoscale transport, mixing, drilling, assembly, and rheology. Our results also establish the fastest reported rotation of a nanomotor in aqueous solution.

KEYWORDS. Acoustic, microvortex, nanomotor, nanoparticle, nanorod, rotation, ultrasonic, ultrasound
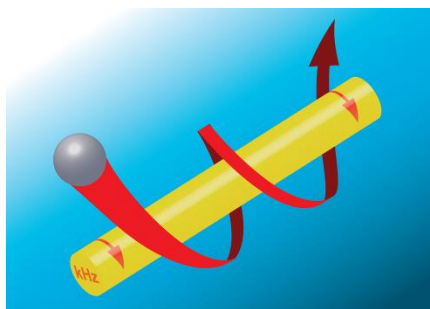
Table of contents graphic. A nanoparticle traces the microvortical flow around a rapidly rotating nanorod propelled by ultrasound.

Nanorods propelled by ultrasound[1] were recently discovered as a dynamic nanotechnology with emerging biomedical applications.[2] In contrast to chemically,[3-6] magnetically,[7, 8] or electrically actuated nanomotors,[9] acoustically actuated nanomotors can transport through aqueous solutions with high ionic strengths and without toxic fuels or external magnetic or electric fields. Such nanomotors can be readily used in living tissue[10] and in combination[11] with other propulsion mechanisms,[12] and have been envisioned[13, 14] for use in exciting applications such as diagnosing disease,[15, 16] delivering drugs,[17] and performing surgery.[18] However, to fulfill the potential of nanomotors propelled by ultrasound for rapidly transporting through and strongly interacting with biological media, the basic dynamics of the nanomotors must be clearly understood.

Such nanomotors, which are typically metallic rods that are a few micrometers in length and a few hundred nanometers in diameter, exhibit several modes of motion in the presence of acoustic actuation. Both translation along and rotation around the principal longitudinal axis (henceforth, translation and rotation) of single nanomotors have been observed, as well as collective motions involving many interacting nanomotors.[2] While translation is an interesting

mode of motion that is relatively straightforward to directly measure, rotation is a particularly

fascinating mode of motion that motivates further study, for several reasons. First, hydrodynamic

interactions of nanomotors with other objects or one another at low Reynolds number *Re* are

determined in part by the vortical flows around nanomotors, which relate to the rates of nanorod

rotation.[19] Interactions among multiple nanomotors[2] may be strongly influenced by such

microvortices, depending on the rotation and flow rates. Second, any correlation, or lack thereof,

between rotation and translation is important for understanding, engineering, and applying these

modes of motion. The deliberate coupling of rotation and translation may provide a mechanism

for propulsion, as is the case for natural[20] and artificial[21] flagella, while the deliberate decoupling

of rotation and translation may enable independent control over these modes of motion, as is

generally necessary for selective transport and rotary tools. Third, rotation is difficult to directly

image for nanomotors that are rapidly rotating and optically featureless around the longitudinal

axis, so that rates of rotation are quantitatively unknown and *potentially* very high, considering

the ultrasonic actuation frequency of a few megahertz. Therefore, the extent of hydrodynamic

interaction with the surrounding environment and any correlation of the modes of motion are

open problems. For these reasons, measuring hydrodynamic interaction and inferring rotational

motion are essential to understanding and using this dynamic nanotechnology.

Here, as illustrated in Fig. 1, we use polystyrene nanoparticles as optical indicators of the

microvortical flows around gold nanorods propelled by ultrasound in an acoustic resonator. We

track the microvortex advection of nanoparticle tracers around rotating and translating

nanomotors by darkfield localization microscopy. We input our measurements of this motion

into a hydrodynamic model to infer the rotational frequencies of the nanomotors. We discuss

simplifying assumptions underlying our analysis, and resulting uncertainties which are relevant

both to our measurements and to future applications of nanomotors. In the planar pressure node

of a half–wavelength layered acoustic resonator driven at $\approx$ 3 MHz with an energy density of

$< 10\,\mathrm{J}\cdot\mathrm{m}^{-3}$, we infer that nanomotors rotate at frequencies of up to $\approx$ 2.5 kHz, or $\approx$

150,000 RPM. This establishes the fastest reported rotation of a nanomotor in aqueous solution,

and corresponds to tangential speeds at nanomotor surfaces of up to $\approx 2.5\,\mathrm{mm}\cdot\mathrm{s}^{-1}$, which are

two orders of magnitude faster than translational speeds of $\approx 20\,\mu\mathrm{m}\cdot\mathrm{s}^{-1}$. We find that rotation

and translation are independent and variable modes of motion within experimental uncertainty.

These surprising results are essential to understanding the behavior of nanomotors propelled by

ultrasound, and this unprecedented combination of small size and fast rotation is highly relevant

to emerging biomedical applications of nanomotors, as well as other applications involving

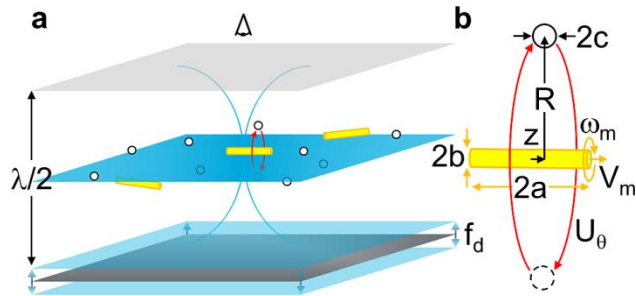nanoscale transport,[22] mixing,[23] drilling,[24, 25] assembly,[26] and rheology.[27]

Figure 1. Schematics illustrating the acoustic actuation of a nanomotor and the microvortex

advection of a nanoparticle. (**a**) A half–wavelength layered acoustic resonator filled with water is

driven at a frequency $f_d \approx$ 3 MHz with an energy density of $< 10\,\mathrm{J}\cdot\mathrm{m}^{-3}$. Gold nanorods are

levitated into and propelled around the planar pressure node of the resonator. Polystyrene

nanoparticles are levitated into the planar pressure node and advected by the microvortical flows

around nearby nanomotors. (**b**) We model a nanomotor as a cylinder of length $2a$ and diameter

$2b$ with the longitudinal axis oriented in the focal plane of an optical microscope. The nanomotor

rotates around the longitudinal axis with an angular speed of $\omega_m = 2\pi f_m$ and translates along

the longitudinal axis with a speed V_m. We model the nanoparticle as a sphere of diameter $2c$ and

diffusivity D, located at a radial distance R from the nanomotor and at a fore and aft position z

from the center along the longitudinal axis of the nanomotor. The nanoparticle is advected with a

tangential speed U_θ.

RESULTS AND DISCUSSION

Motivation

Acoustic actuation is a popular method for manipulating small objects in liquids,[1] and the

recent discovery of the propulsion of metallic nanorods by ultrasound[2, 12, 28] has generated

growing interest in the use of such nanomotors for interacting with biological media. However,

the basic dynamics of these nanomotors, and the resulting hydrodynamic interactions between

nanomotors and other small objects, are not clearly understood. Such dynamics and interactions

may be probed by imaging the motion of tracer particles and thus visualizing the flow fields

around objects of interest. Flow fields around motile bacterial swimmers have been studied[29, 30]

in this way to better understand swimming mechanisms and hydrodynamic interactions between

bacteria. Inspired by natural swimmers,[31] artificial motors have been recently developed[7, 21] for

inducing fluid flows and transporting bacteria and other microscale objects by hydrodynamic

interactions.[32] However, controlling and measuring dynamics and interactions at low Re becomes

increasingly challenging as the dimensions of nanoscale objects become less uniform and as the

motion of nanoscale objects become less deterministic and more stochastic.[6] Our

multidisciplinary study therefore combines ultrasonic actuation, low Re fluid dynamics and

hydrodynamic interactions, nanoscale control and fluctuations, and measurement science in an approach towards understanding the behavior of this dynamic nanotechnology.

Analytical approach

We measure the microvortex advection of a tracer nanoparticle around a nanomotor, input our measurements into a hydrodynamic model of this interaction, and in this way infer the rotational frequency of the nanomotor. Our approach relies on several simplifying approximations – including that of a Stokes flow around a nanomotor, that only hydrodynamic forces from a microvortical flow act on a nanoparticle, and that nanomotors and nanoparticles are, respectively, perfectly cylindrical and spherical in shape – and thus ignores a description of the actual cause of such motion. We describe and justify these simplifying assumptions in the Supporting Information. A complete theoretical model of the acoustic actuation of nanomotor rotation and translation is beyond the scope of our study. However, the eventual development of such a model must be consistent with our novel experimental results. In particular, we measure a relation between the tangential speed of a nanoparticle advecting around a rotating nanomotor and radial distance between the pair that is reasonably well described by a hydrodynamic interaction,[19] which must be explained by any, more detailed, model of the system.

Microvortical flow

We use an analytical expression derived by Chwang and Wu[19] to model the vortical flow at low *Re* around a slender axisymmetric body rotating around its longitudinal axis. The following expression applies in the limiting case of a long rod, which is a good approximation for our experimental nanorod length to diameter aspect ratio of ≈ 7, as shown in Fig. 2. If the measured tangential speed of the vortical flow as indicated by a tracer nanoparticle is U_θ, then

$$U_\theta \approx \frac{\omega_m b^2}{2R}\left[\frac{z+a}{\sqrt{(z+a)^2+R^2}} - \frac{z-a}{\sqrt{(z-a)^2+R^2}}\right]. \qquad \text{EQUATION (1)}$$

The other variables in this expression are as follows: ω_m is the inferred angular speed of the nanomotor, which we also discuss as a rotational frequency $f_m = \frac{\omega_m}{2\pi}$; R is the measured radial distance between the center of a tracer nanoparticle and the center of a nanomotor; z is the measured fore and aft position of the tracer nanoparticle from the center along the longitudinal axis of the nanomotor; and $2a$ and $2b$ are the measured length and diameter of the nanomotor, respectively. This expression is independent of viscosity in the limit of a quasi–static Stokes flow. This model has been experimentally validated for objects with dimensions on the order of hundreds of micrometers,[33] and is further tested for the rotating nanomotors studied here. Nanomotor translation also induces a flow field which we estimate to be relatively insignificant, while *a posteriori* estimates of Re and viscous penetration depth are consistent with our assumption of a quasi–static Stokes flow, as described below and in the Supporting Information.
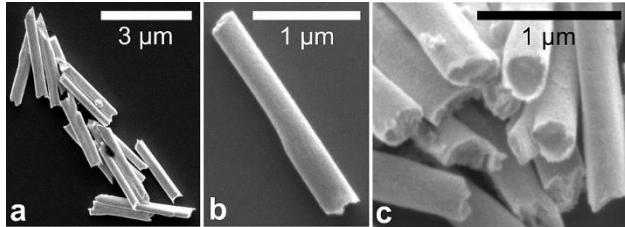

Figure 2. Scanning electron micrographs showing the sizes and shapes of gold nanorods. (**a**) The ensemble of nanorods has lengths of $2a = (2.19 \pm 0.28)$ µm and diameters of $2b = (316 \pm 39)$ nm (average ± standard deviation, $N = 20$), yielding an average length to diameter aspect ratio of ≈ 7. (**b**) Individual nanorods show variation in diameter, (**c**) end shape and surface roughness.

Tracer considerations

We trace the flow field around a nanomotor by imaging the microvortex advection of a nanoparticle. The size of the nanoparticle and proximity to the nanomotor must be chosen such

that the nanoparticle serves as both a passive and precise indicator of the flow field. Several competing experimental considerations inform our semi–empirical selection of nanoparticle hydrodynamic radius of $c \approx 200$ nm and radial distance of $R > 1$ µm. The flow field is perturbed less by a smaller nanoparticle that is further from the nanomotor. Conversely, a larger nanoparticle that is closer to the nanomotor exhibits less stochastic diffusion and is advected more deterministically. A larger nanoparticle also scatters more light in darkfield microscopy and can be localized more precisely.

The maximum size and minimum proximity of a tracer nanoparticle is limited by the fractional hydrodynamic perturbation to the nanomotor rotation from the wake of a nanoparticle, $\delta_f = \left| \frac{f_0 - f_{pert}}{f_0} \right|$, where f_{pert} and f_0 are, respectively, the perturbed and unperturbed nanomotor rotational frequencies. We estimate a range of values for δ_f using two far field approximations, both based on a single iteration of the method of reflections.[34] Details of these calculations are presented in the Supporting Information. In a deliberate overestimate of the perturbation, we artificially impose an external force to hold a nanoparticle stationary in the flow field described by Eqn. 1, and we calculate the perturbation from this additional Stokes drag. In the far field, the actual perturbation is smaller than this overestimate, which yields a perturbation of $\delta_f < 2$ % for $R > 1$ µm, as shown in Fig. S1. This analysis is informative for emerging applications of nanomotors hydrodynamically interacting with other small objects, such as cellular organelles,[10] that may be constrained in a biological media. In a realistic estimate of the perturbation, with no external forces and torques, the fluid flow incident on an ideal tracer will, in the Stokes approximation, transport the tracer with the same velocity and angular velocity as the average flow field at the tracer.[9] In this case, we treat the perturbation δ_f as being due only to nanoparticle rotation, using the approximation of a tracer in a linearly varying velocity flow field

in the radial direction. This analysis yields a perturbation of $\delta_f < 0.5$ % for $R > 1$ µm, as shown in Fig. S1, which is negligibly small compared to the other sources of uncertainty in our measurements described below. Therefore, the nanoparticles qualify as effectively noninteracting tracers of microvortical flows in our study.

Conversely, the minimum size and maximum distance of a tracer nanoparticle is limited by the stochastic diffusion of a nanoparticle, contributing uncertainty to a measurement of the deterministic advection of the nanoparticle by the flow field and thus U_θ and R. A nanoparticle is only useful as a tracer in our measurements if the rate of advection significantly exceeds the rate of diffusion. The relative rates of advection and diffusion are compared by the Brenner number $Br = U_\theta R / \pi D$, where D is the measured diffusion coefficient of the nanoparticle tracer, expressed through the Stokes-Einstein relation as $D = k_B T / 6\pi\eta c$, where k_B is the Boltzmann constant, T is the absolute temperature of the aqueous solution, and η is the dynamic viscosity. Due to the fast microvortical flows around nanomotors, we measure typical values of $Br \gtrsim 10$ and a typical relative standard uncertainty in U_θ of < 5 %, quantifying our extent of hydrodynamic control over the transport of nanoparticles, and satisfying our need for quasi–deterministic nanoparticle transport in our measurements.

Independent motions

In the absence of acoustic actuation, polystyrene nanoparticles randomly diffuse throughout the sample volume, while gold nanorods randomly diffuse and eventually sediment onto the matching layer of the acoustic resonator. In the presence of acoustic actuation, both polystyrene nanoparticles and gold nanorods levitate into and concentrate around the planar pressure node of the acoustic resonator,[35] as illustrated in Fig. 1. Polystyrene nanoparticles continue to diffuse randomly and are advected to varying extents, possibly by acoustic

streaming, around the planar pressure node of the resonator. Independently of interactions with nanomotors, nanoparticles diffuse at the same rate of $D = (1.04 \pm 0.14)\ \mu m^2 \cdot s^{-1}$ (average $\pm$ standard uncertainty) before, during, and after acoustic actuation. Individual gold nanorods are propelled throughout the planar pressure node of the acoustic resonator with significant variation in translational speed, path, and concentration, as demonstrated previously.[2] Fig. 3 shows representative data of nanoparticle diffusion, nanomotor propulsion, and nanoparticle advection.
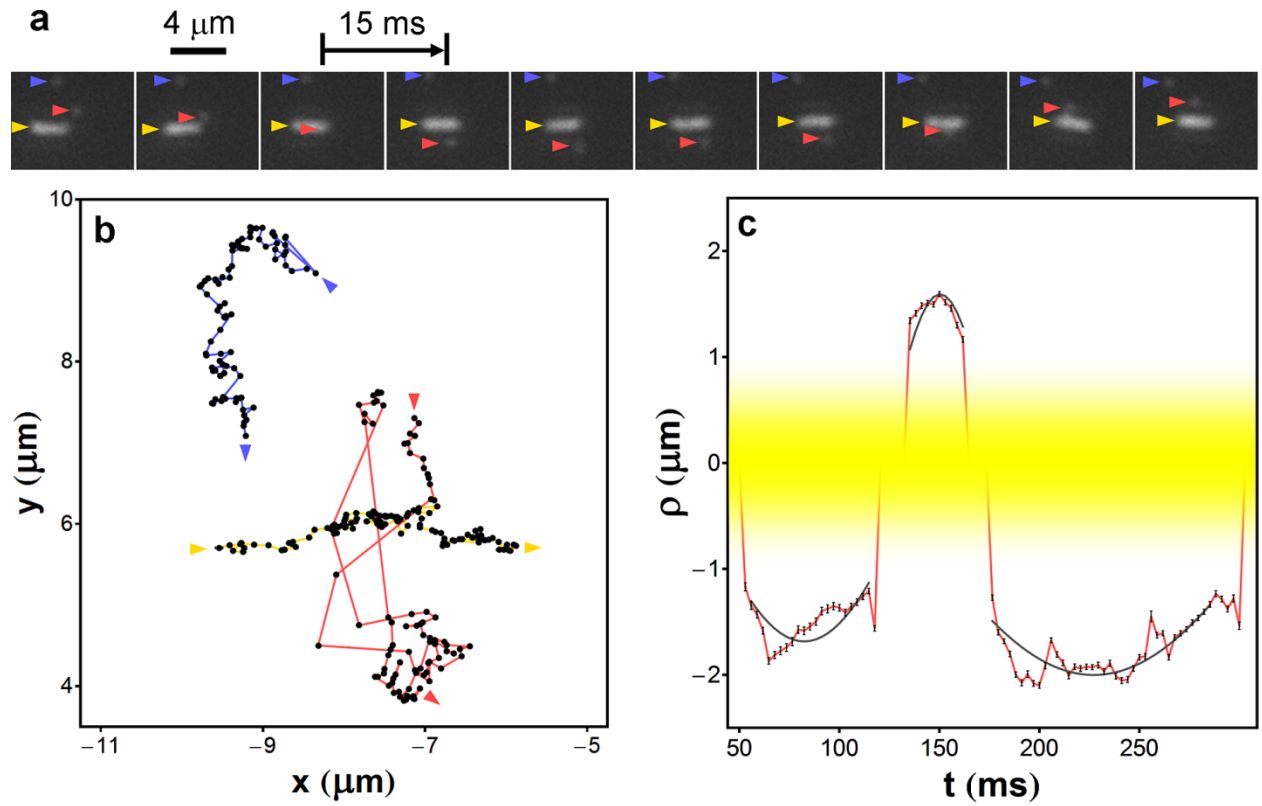

Figure 3. Representative data showing the measurement and analysis of the motion of a nanomotor and two nanoparticles. (**a**) Darkfield micrographs show projections in the image plane of nanoparticle diffusion as indicated by blue arrows, nanomotor propulsion as indicated by gold arrows, and nanoparticle advection for $\approx 2\pi$ radians as indicated by red arrows. Sequential video frames are advanced in time by ≈ 15 ms from left to right. (**b**) Nanomotors and

nanoparticles are localized in each video frame. Sequential data points are advanced in time by

≈ 3 ms, and trajectories in the camera coordinate frame are plotted as color coded lines with

arrows indicating the direction of motion. (**c**) The trajectory of the nanoparticle is transformed

into the coordinate frame of the nanomotor. Projected radial distance ρ as a function of time t is

modeled as a sinusoidal function, shown as a gray line, to extract tangential speed U_θ and radial

distance R between multiple frames of a video. The nanomotor occults the nanoparticle around

$\rho \approx 0$, as indicated by the gold blur. Vertical and horizontal bars are one standard uncertainty

and are smaller than the data markers in some cases.

Microvortex advection

   Previously, microvortical flows among ensembles of nanomotors and nanoparticles were

qualitatively observed.[2] Here, we *quantitatively* analyze the microvortex advection of single

nanoparticles around single nanomotors propelling randomly past, as shown in Fig. 3 and in Vid.

S1. Absent a nearby nanomotor, nanoparticles diffuse randomly and exhibit minimal advection

by acoustic streaming. Importantly, we observe the microvortex advection of nanoparticles *only*

as nanomotors transit in close proximity, and we do not observe the microvortex advection of

nanoparticles without a nanomotor nearby. These observations demonstrate that the microvortex

advection of a nanoparticle is a result of the hydrodynamic interaction with a nanomotor, and is

not a result of any primary acoustophoretic streaming field in the acoustic resonator, as described

in the Supporting Information. The microvortex advection of nanoparticles is evident in the

majority of close encounters with nanomotors, indicating that most of these nanomotors have

associated microvortical flows. However, due to the large distribution of approach distances

between individual nanomotors and nanoparticles, particle tracking in three dimensions is needed

to quantify the fraction of rotating nanomotors. We categorize microvortex advection for analysis by the persistence of nanoparticle entrainment, measured in units of radians around the longitudinal axis. While some advection events persist for $< \pi$ radians, others persist for up to $\approx 8\pi$ radians, as shown in Vid. S2. This variability in persistence is due to the stochastic diffusion of both nanomotors and nanoparticles, as well as variation in approach distances and translational and rotational speeds of nanomotors, as described below. We quantitatively analyze only those nanoparticles entrained in a microvortex for $\geq 2\pi$ radians, as shown in Fig. 3a, as such events allow for more reliable tracking of nanoparticle motion. Highly persistent microvortex advections enable repeated measurements of the rotation of individual nanomotors and are therefore particularly interesting for quantitative analysis.

We extract values of U_θ, R, and z from each microvortex advection event of $\geq 2\pi$ radians, as shown in Fig. 3 and Fig. S3. We assume constant values of U_θ and R during a circular trajectory of a nanoparticle around a nanomotor, occurring at large enough Br. Details of this analysis are described in the Methods and in the Supporting Information. Fig. 4 shows these measured quantities from the increasingly persistent microvortex advection of four nanoparticles around four nanomotors. The data points in Fig. 4a correspond to the nanomotor shown in Figure 3, while the data points in Figs. 4b–d corresponds to other nanomotors. Each microvortex advection event is plotted to the scale of the nanoparticles and color coded to U_θ, with 5 µm · s^{-1} gradations in color conservatively representing the standard uncertainty in U_θ. Variations in z are due to nanomotor propulsion and diffusion along the longitudinal axis, as well as diffusion of nanoparticles, during microvortex advection. U_θ varies over different ranges for the four nanomotors, indicating variation in microvortical flow rates but making it difficult to discern a trend in Fig. 4 and motivating additional testing of our measurement method before returning to

an analysis of the rates of rotation of individual nanomotors. We analyze a total of 9 individual nanomotors to obtain 41 total individual microvortex advections.
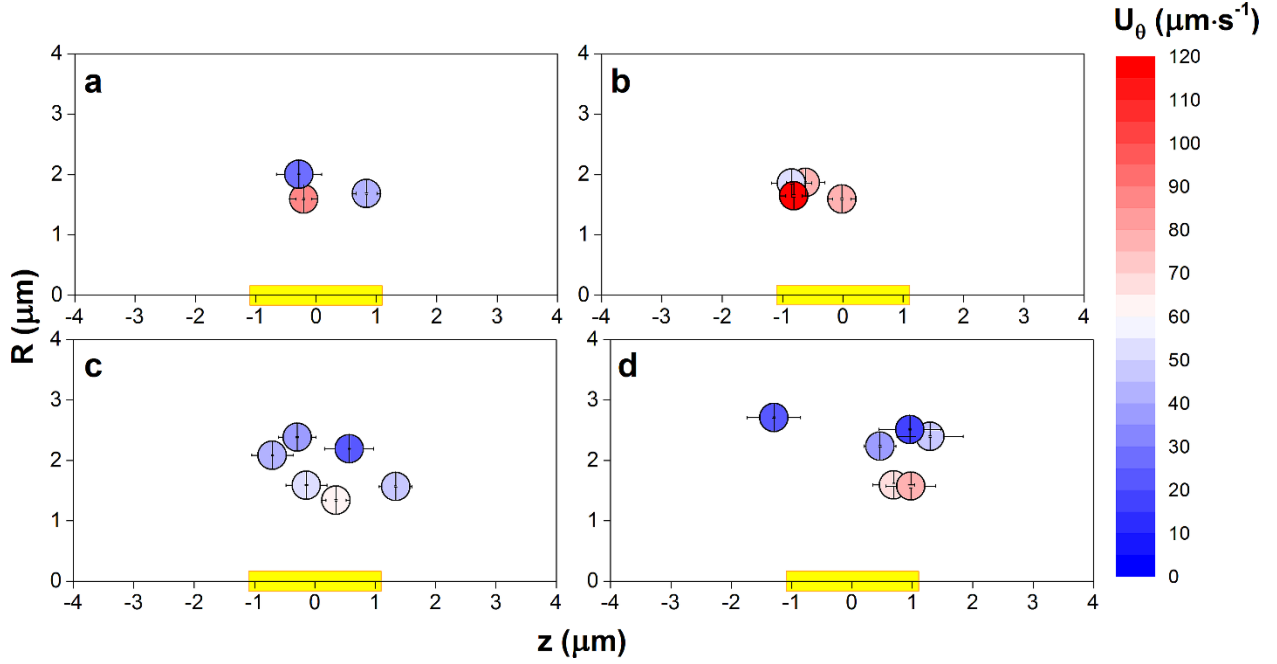

Figure 4. Representative data showing four microvortex advection events of varying speed and increasing persistence. The data points in (**a**) correspond to the nanomotor shown in Figure 3, while the data points in (**b**), (**c**), and (**d**) correspond to other nanomotors. Variation in the ranges of tangential speed U_θ indicates different microvortical flow speeds around the individual nanomotors driven by different rotational frequencies f_m. Nanoparticles are shown to scale and color coded to U_θ, with $5 \, \mu m \cdot s^{-1}$ gradations in color conservatively representing the standard uncertainty of U_θ. Vertical and horizontal bars are one standard uncertainty of radial distance R and one standard deviation of fore and aft position z, respectively, as nanomotors translate and diffuse along the longitudinal axis during microvortex advection. Nanorods are illustrated approximately to scale.

Model test

We test the validity of Eqn. 1 to infer values of $\omega_m = 2\pi f_m$ from our experimental measurements. To do so, we fit the experimental relation between *all* measurements of U_θ and R to Eqn. 1, using average values of a, b, and z, while leaving ω_m as a free parameter. The fit has an adjusted $R^2 = 0.86$ and is shown as a grey line in Fig. 5, demonstrating reasonable agreement between the expected $U_\theta(R)$ relation and the ensemble experimental data, and, in this way, supporting our use of a hydrodynamic model of the interaction between a nanomotor and a nanoparticle. Significant scatter of the data is evident, resulting from variation in the rotational frequencies and dimensions of individual nanomotors, and in fore and aft position during microvortex advection due to nanomotor diffusion and propulsion. The left side of Fig. 5 shows tangential surface speeds at the average nanomotor radius of $b \approx 160$ nm for individual microvortex advection events, as inferred using Eqn. 1. These individually inferred values, with an average tangential surface speed of ≈ 1.5 mm $\cdot$ s^{-1}, are consistent with the fit relation from the ensemble experimental data.
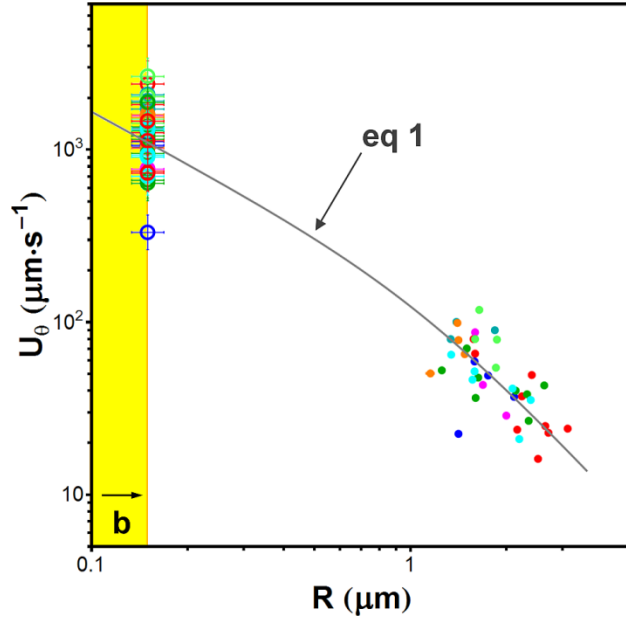
Figure 5. We test the validity of Eqn. 1 to infer nanomotor rotational frequency from the microvortex advection of tracer nanoparticles. We fit the experimental relation between tangential speed U_θ and radial distance R to Eqn. 1, using average values of length $2a$, diameter $2b$, and fore and aft position z, while leaving angular speed $\omega_m = 2\pi f_m$ as a free parameter. The fit has an adjusted $R^2 = 0.86$ and is shown as a gray line, demonstrating reasonable agreement between theory and experiment. Repeated measurements of the persistent microvortex advection of tracer nanoparticles around individual nanomotors are color coded. Individually inferred values of f_m and derived nanomotor surface tangential speeds, shown as open circles, are consistent with the fit relation from the ensemble experimental data. Vertical and horizontal bars are one standard uncertainty and may be smaller than the data points.

Uncertainty propagation

Each of the five variables that we input into Eqn. 1; U_θ, R, z, a and b, has an associated uncertainty which is propagated through to the inferred value of ω_m. It is worth examining the relative importance of these uncertainties for the purposes of better understanding our inference

of rotational frequency and of informing future applications of nanomotors. We begin by inputting into Eqn. 1, average values of $2a$ and $2b$ with standard deviation values obtained from scanning electron microscopy treated as measurement uncertainties on an ensemble basis. Fig. 6 shows, in this case, the resulting contributions of each of the five variables to the total uncertainty in $f_m = \omega_m/2\pi$ as histograms. It is apparent from Fig. 6 that, if the lengths and diameters of nanomotors cannot be characterized on an individual basis, as is the case for our experimental study and presumably for many applications of nanomotors, then the statistical distributions of these values dominate the uncertainty in a measurement of nanomotor rotation, accounting for $> 85\ \%$ of the total uncertainty. The polydispersity in nanorod dimensions, $2a = (2.19 \pm 0.28)$ µm and $2b = (316 \pm 39)$ nm (average $\pm$ standard deviation, $N = 20$), is a result of the electrodeposition process guided by a nanoporous template that we use to fabricate the gold nanorods, emphasizing that nanoscale dimensional control over nanorod structure is critical in future applications of nanomotors. As a final note on the propagation of measurement uncertainty, the relatively small contribution of U_θ and R to the total uncertainty in an estimate of f_m validates our semi-empirical selection of tracer nanoparticle size and proximity.
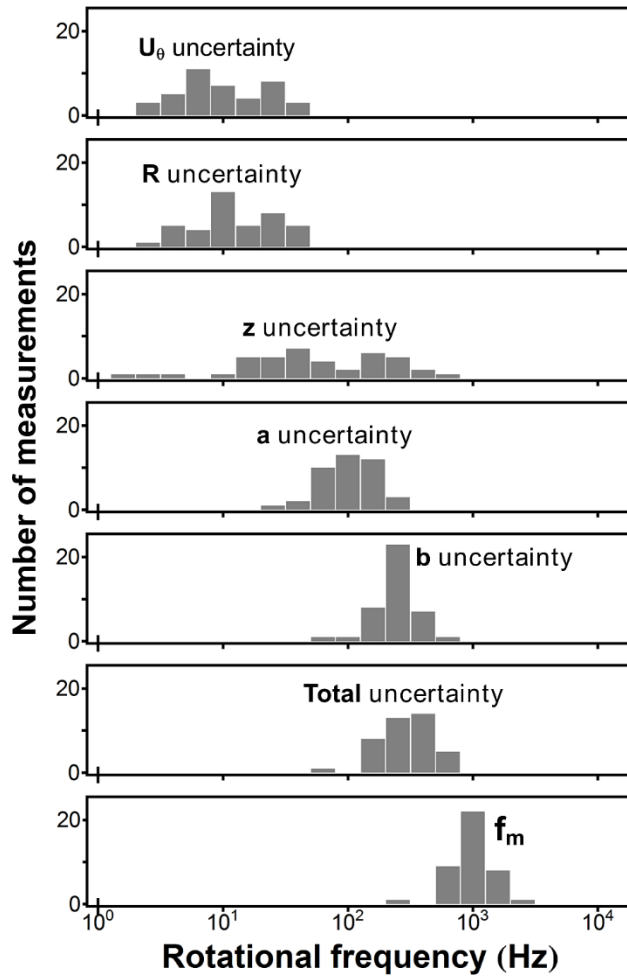
Figure 6. An analysis of measurement uncertainty elucidates our inferences of kilohertz rotation and informs future applications of nanomotors. Each of the five measured values input into Eqn. 1 contributes differently to the total uncertainty in rotational frequency f_m. The various contributions are plotted as histograms, in the case that nanomotor length $2a$ and diameter $2b$ are characterized as an ensemble average and standard deviation. The distributions of nanorod length, $2a = (2.19 \pm 0.28)$ μm, and nanorod diameter, $2b = (316 \pm 39)$ nm, (average $\pm$ standard deviation, $N = 20$), result in > 85 % of the total uncertainty in f_m, demonstrating that dimensional control is critical in future applications of nanomotors.

Rotation inference

With our hydrodynamic model tested and our measurement uncertainty characterized, we analyze our inferences of the rotation of individual nanomotors. We study, for example, the persistent microvortex advection of tracer nanoparticles around the two nanomotors shown in Figs. 4c and 4d. Individual estimates of rotational frequency and measurement uncertainty, as well as the statistical variation of these values, are tabulated in Table S1 of the Supporting Information. Differences between repeated inferences of the rotational frequency of an individual nanomotor over a time scale of $\approx$ 100 ms are often within, but occasionally exceed, the measurement uncertainty. Similarly, the variation in rotational frequency between different nanomotors exceeds the measurement uncertainty in some instances. Differences between the rotational frequencies of individual nanomotors may be attributed to heterogeneity in nanomotor structure and the resulting transduction of acoustic energy into motion, as well as any lateral variation in acoustic energy density around the planar pressure node of the acoustic resonator. Nanomotors rotate with a broad distribution of inferred frequencies ranging from $f_m \approx$ (0.5 to 2.5) kHz, as shown in Fig. 6. For nanorods with radii of $b \approx 160$ nm, these inferred rotational frequencies correspond to Reynolds number $Re < 10^{-3}$ and viscous penetration depths of > 8 µm, which are consistent with our assumption of a quasi–static Stokes flow,[36] as described in the Supporting Information.

Rotation and translation

We compare inferred rotational frequencies f_m to measured translational speeds V_m of individual nanomotors during the microvortex advection of tracer nanoparticles. We analyze the correlation between f_m and V_m to determine if rotation and translation are dependent or independent modes of motion. It seems evident in Fig. 7 that rotation and translation are

independent and variable. Noting that we do not know the direction of nanomotor rotation or the polarity of any coupling between rotation and translation, we calculate adjusted R^2 values for $f_m(|V_m|)$ such that our analysis is sensitive to any existing correlation. We find an adjusted R^2 value for $f_m(|V_m|)$ that is similar to that of randomly generated data, demonstrating that, within the uncertainty of our measurements, rotation and translation are independent modes of motion in our experimental system.
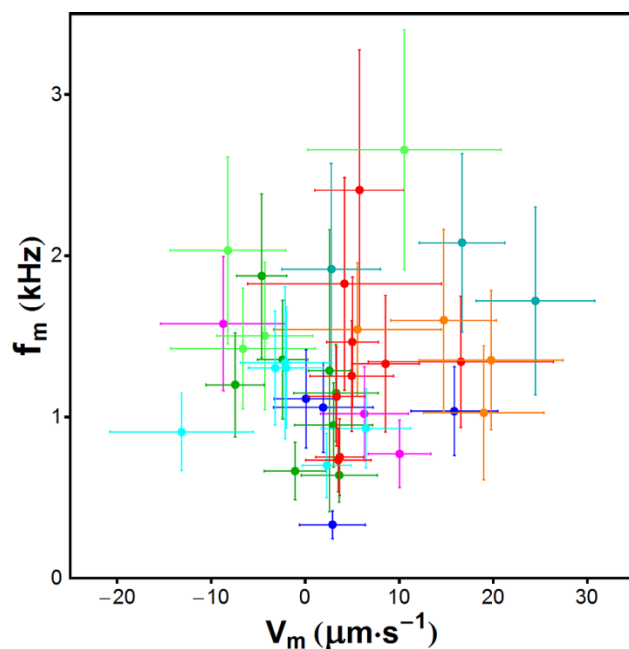

Figure 7. Nanomotor rotation and translation are independent and variable modes of motion. Individual nanomotors are coded by different colors maintained from Fig. 5. The resulting data points are scattered with rotation and translation uncorrelated, even for an individual nanomotor during persistent microvortex advection. Vertical and horizontal bars are one standard uncertainty. Uncertainty in rotational frequency f_m is dominated by the polydispersity of nanorod dimensions, while uncertainty in translational speed V_m is dominated by diffusion along the longitudinal axis of the nanomotors.

CONCLUSIONS

The field of nanomotors propelled by ultrasound is rapidly developing, so that understanding the dynamics and interactions of these devices is becoming increasingly important for advancing novel applications and understanding potential limitations. Our study provides the first measure of the microvortical flows around rotating and translating gold nanorods propelled by ultrasound. We input our measurements into a simplified hydrodynamic model to infer the rotational frequencies of nanomotors. In the planar pressure node of a half–wavelength layered acoustic resonator driven at ≈ 3 MHz and with an energy density of < 10 J $\cdot$ m^{-3}, we infer that gold nanorods rotate around the longitudinal axis at frequencies of up to ≈ 2.5 kHz, or $\approx$ 150,000 RPM, corresponding to tangential surface speeds of up to ≈ 2.5 mm $\cdot$ s^{-1}. This is the fastest reported rotation of a nanomotor in aqueous solution, exceeding a recently reported record value[9] by an order of magnitude. Nanomotors also translate along the longitudinal axis at speeds of up to ≈ 20 μm $\cdot$ s^{-1} in our experimental system. The even faster translation of up to $V_m \approx$ 200 μm $\cdot$ s^{-1} of similar nanomotors in a previous study is likely due to the use of an acoustic resonator with a similar input power but a higher quality factor,[2] indicating the possibility of nanomotor rotation faster than ≈ 2.5 kHz. We find that the majority of randomly propelling nanomotors have associated microvortical flows, independently of translational speed or coupling between nanomotors.

These results suggest several future studies. We hypothesize that microvortical flows could mediate the attraction or repulsion of multiple nanomotors in a manner that is analogous to the interaction of magnetic fields resulting from multiple magnetic dipoles, due to the similarity of the underlying equations. Future study is required to test our hypothesis, as well as to clarify

the actuation mechanisms for rotation and translation. Precisely nanofabricated structures, combined with the measurement methods and results that we report here, would be helpful in this regard. The longitudinal asymmetries of the concavity of the ends of a nanorod and of the angle of a nanorod relative to the planar pressure node have been implicated in nanomotor translation[2, 12] and rotation,[2] respectively. The kilohertz rotation of nanomotors indicates that axial asymmetry, in particular helicity, is a relevant structural characteristic to further control and investigate. Interestingly, rotation and translation are *not* coupled through any helicity of our nanorods, indicating different acoustic actuation mechanisms driving the two modes of motion, and suggesting the future possibility of deliberately decoupling and separately controlling rotation and translation. Beyond the basic issue of selectively transporting nanomotors by translation and inducing microvortical flows by rotation, decoupling rotation and translation is essential in future applications of nanomotors as rotary tools, which generally require independent control over speed and feed. Conversely, recent reports of the fabrication and actuation of metallic helices with dimensions that are similar to our nanorods also suggest the future possibility of deliberately coupling rotation and translation propelled by ultrasound.[7, 21, 37-41]

This unprecedented combination of small size and fast rotation could lead to important advances in biomedical and other applications of nanomotors propelled by ultrasound. For example, our results quantify how nanomotors with associated microvortical flows can quasi–deterministically control the transport of other objects by rapid advection, despite the high rates of stochastic diffusion of nanoscale objects. The enhanced mixing of liquids at low Re[23] follows naturally from our results, while nanoscale drilling, assembly,[26] and rheology[27] are also possibilities with nanomotor rotation occurring at kilohertz frequencies. However, our

measurements also show that future applications would be limited by precise control over the nanoscale dimensions of individual nanomotors. Moreover, our results indicate that such applications should not be predicated on assumed steady state motion or correlation between the rotation and translation of nanomotors.

METHODS

Acoustic resonator

We perform our experiments in a half–wavelength layered acoustic resonator. A ceramic piezoelectric transducer with a thickness of $\approx$ 620 μm and a diameter of $\approx$ 12 mm is adhered by an epoxy coupling layer with a thickness of (9 ± 4) μm (average $\pm$ standard deviation) to the unpolished back side of a silicon matching layer with a thickness of (430 ± 1) μm (average $\pm$ standard deviation), a width of $\approx$ 20 mm, and a length of $\approx$ 25 mm. A polydimethylsiloxane (PDMS) gasket with a thickness of $\approx$ 250 μm, a width of $\approx$ 5 mm, and a length of $\approx$ 10 mm is reversibly bonded to the polished front side of the silicon matching layer, setting the fluid layer thickness. The resonator volume of $\approx$ 0.8 μL is formed by a circular hole with a diameter of $\approx$ 2 mm in the PDMS gasket, into which the sample solution is pipetted. A borosilicate coverslip with a thickness of $\approx$ (160 to 190) μm and a width and length of $\approx$ 18 mm is reversibly bonded to the top of the PDMS gasket as the reflecting layer. We drive the piezoelectric transducer with a sinusoidal function of amplitude from (5 to 10) V and frequency from (2.75 to 3.10) MHz. The conditions for forming a standing wave in the resonator are described by

$$t_{fl} = \frac{1}{2} n \, \lambda = \frac{1}{2} n \left(\frac{c_w}{f_d} \right), \qquad \text{EQUATION (2)}$$

where t_{fl} is the thickness of the fluid layer, n is the number of nodes, λ is the wavelength of sound in the fluid, c_w is the speed of sound in water, and f_d is the driving frequency of the

piezoelectric transducer. For a layered resonator with a single node operating at values of f_d from (2.75 to 3.10) MHz, the ideal value of t_{fl} respectively varies from (240 to 270) μm. We tune f_d for each experiment to accommodate variation in PDMS gasket thickness and borosilicate coverslip thickness. We measure an electrical input power of < 1 W over the entire piezoelectric transducer area of 113 mm^2. In the presence of acoustic actuation, nanomotors and nanoparticles levitate into a band with a thickness of several micrometers near the vertical mid-plane of the resonator, with nanomotors typically oriented with the longitudinal axis in this plane.

Nanorod properties

We fabricate gold nanorods by an electrodeposition process guided by a nanoscale porous alumina template.[42] We characterize the sizes and shapes of individual nanorods by scanning electron microscopy, as shown in Fig. 3. The nanorods, as an ensemble, have dry diameters of (316 ± 39) nm and lengths of (2.19 ± 0.28) μm (average $\pm$ standard deviation, $N = 20$), with individual nanorods showing variation in end shape and surface roughness. We load gold nanorods into the sample cell at a volume fraction of $\approx 10^{-5}$.

Nanoparticle properties

We use polystyrene spheres with wet diameters of (390 ± 12) nm (average $\pm$ standard deviation, as measured by the manufacturer using a disc centrifuge; the average value is traceable to the National Institute of Standards and Technology) to trace the flow fields induced by rotating nanomotors. Such nanoparticles serve as good tracers for several reasons beyond the considerations discussed above guiding our selection of nanoparticle size. While an ideal tracer would have the same density as water, polystyrene is only ≈ 5 % denser than deionized water, and such nanoparticles can be obtained commercially with nearly monodisperse size distribution,

highly regular spherical shapes, and relatively smooth surfaces. We load polystyrene nanoparticles into the sample cell at a volume fraction of $\approx 10^{-5}$.

Optical microscopy

We image the motion of nanomotors and nanoparticles by darkfield microscopy. To balance collection efficiency, field of view, and depth of field, we use an air immersion objective lens with corrections for flat field and chromatic aberrations, a magnification of $50 \times$, and a numerical aperture of 0.80. The depth of field of ≈ 1.2 µm is collocated with the planar pressure node of the acoustic standing wave near the vertical midplane of the acoustic resonator. The polished front side of the silicon matching layer provides low background light scattering for high optical signal to noise ratio. Images are collected at a frame rate of ≈ 338 s^{-1} using a scientific complementary metal–oxide–semiconductor (sCMOS) camera with an on–chip pixel size of 6.5 µm. Videos are typically acquired in 8×10^3 frame segments composed of 5×10^2 initial frames immediately before acoustic actuation, 7×10^3 intermediate frames during acoustic excitation, and 5×10^2 final frames immediately after acoustic excitation.

Motion analysis

We analyze the motion of nanomotors and nanoparticles by modeling the two dimensional images of three dimensional objects and motions, localizing and orienting nanomotors and nanoparticles within video frames, and tracking the motion of nanomotors and nanoparticles between video frames.

Nanomotors and nanoparticles are first localized within each video frame, and frames showing interactions between nanomotors and nanoparticles are spatially and temporally cropped. A region of interest (ROI) is centered around a nanomotor as the brightest and largest feature within the ROI. This feature is fit to four spatially offset error functions to determine both

the position and orientation of the nanomotor. The residual of this fit is obtained to isolate the nanoparticle. This brightest and largest feature in this residual ROI is fit to a two dimensional, radially symmetric Gaussian function to obtain the nanoparticle position. Details of this analysis are presented in the Supporting Information.

Nanoparticles and nanomotors are then tracked between multiple frames of a video. The nanomotor position as a function of time data is fit to a linear function to extract the average value of V_m in the image plane. To extract average values of U_θ and R and from the microvortex advection of a nanoparticle around a nanomotor, the measured trajectory is modeled as a sinusoidal function, as shown in Fig. S3, projecting circular motion in three dimensions to images in two dimensions and assuming constant U_θ and R for microvortex advection, at large enough Br. Details of this analysis are presented in the Supporting Information.

In these analyses, measurement uncertainties are determined as the standard uncertainties of the fitted values of position, orientation, and speed, and are propagated throughout the algorithm and subsequent calculations. Nanomotors and nanoparticles are localized with typical standard uncertainties of ≈ 50 nm and ≈ 100 nm, respectively. Limited photon count and motion blur both contribute uncertainty to localization and tracking.

Independently of hydrodynamic interactions with nanomotors, we analyze the stochastic diffusion of nanoparticles before, during, and after acoustic actuation. We localize individual nanoparticles over 500 frames and compute the two dimensional mean squared displacement MSD as a function of time. We measure D from the slope of a linear fit to $MSD(t)$ for individual nanoparticles. We then use the known value of the nanoparticle radius c and the known lumped parameter of $\frac{T}{\eta(T)}$ for water[43] with the Stokes–Einstein relation to estimate an aqueous solution temperature of $T = (295 \pm 5)$ K (average ± standard uncertainty) before, during, and after

acoustic actuation. This value is consistent with the ambient experimental temperature of

$\approx$ 295 K.

SUPPORTING INFORMATION

Details of simplifying assumptions, perturbation estimates, image analysis, tracking analysis, and

representative videos are available free of charge on the Internet at http://pubs.acs.org.

REFERENCES:

1.   Friend, J.; Yeo, L. Y. Microscale Acoustofluidics: Microfluidics Driven *via* Acoustics

and Ultrasonics. *Rev. Mod. Phys.* **2011**, 83, 647-704.

2.   Wang, W.; Castro, L. A.; Hoyos, M.; Mallouk, T. E. Autonomous Motion of Metallic

Microrods Propelled by Ultrasound. *ACS Nano* **2012**, 6, 6122-6132.

3.   Paxton, W. F.; Kistler, K. C.; Olmeda, C. C.; Sen, A.; St. Angelo, S. K.; Cao, Y.;

Mallouk, T. E.; Lammert, P. E.; Crespi, V. H. Catalytic Nanomotors: Autonomous Movement of

Striped Nanorods. *J. Am. Chem. Soc.* **2004**, 126, 13424-13431.

4.   Demirok, U. K.; Laocharoensuk, R.; Manesh, K. M.; Wang, J. Ultrafast Catalytic Alloy Nanomotors. *Angew. Chem., Int. Ed.* **2008**, 47, 9349-9351.

5.   Sailapu, S. K.; Chattopadhyay, A. Induction of Electromotive Force by an Autonomously Moving Magnetic Bot. *Angew. Chem., Int. Ed.* **2014**, 53, 1521-1524.

6.   Lee, T.-C.; Alarcón-Correa, M.; Miksch, C.; Hahn, K.; Gibbs, J. G.; Fischer, P. Self-Propelling Nanomotors in the Presence of Strong Brownian Forces. *Nano Lett.* **2014**, 14, 2407-2412.

7.   Ghosh, A.; Fischer, P. Controlled Propulsion of Artificial Magnetic Nanostructured Propellers. *Nano Lett.* **2009**, 9, 2243-2245.

8.   Gao, W.; Kagan, D.; Pak, O. S.; Clawson, C.; Campuzano, S.; Chuluun‑Erdene, E.; Shipton, E.; Fullerton, E. E.; Zhang, L.; Lauga, E. Cargo‑Towing Fuel‑Free Magnetic Nanoswimmers for Targeted Drug Delivery. *Small* **2012**, 8, 460-467.

9.   Kim, K.; Xu, X.; Guo, J.; Fan, D. L. Ultrahigh-Speed Rotating Nanoelectromechanical System Devices Assembled From Nanoscale Building Blocks. *Nat. Commun.* **2014**, 5.

10.   Wang, W.; Li, S.; Mair, L.; Ahmed, S.; Huang, T. J.; Mallouk, T. E. Acoustic Propulsion of Nanorod Motors Inside Living Cells. *Angew. Chem., Int. Ed.* **2014**, 126, 3265-3268.

11.   Dong, B.; Zhou, T.; Zhang, H.; Li, C. Y. Directed Self-Assembly of Nanoparticles for Nanomotors. *ACS Nano* **2013**, 7, 5192-5198.

12.   Garcia-Gradilla, V.; Orozco, J.; Sattayasamitsathit, S.; Soto, F.; Kuralay, F.; Pourazary, A.; Katzenberg, A.; Gao, W.; Shen, Y. F.; Wang, J. Functionalized Ultrasound-Propelled Magnetically Guided Nanomotors: Toward Practical Biomedical Applications. *ACS Nano* **2013**, 7, 9232-9240.

13.   Ju, H.; Zhang, X.; Wang, J. Nanobiosensing for Clinical Diagnosis. In *NanoBiosensing*, Springer: 2011; pp 535-567.

14.   Wang, J. Can Man-Made Nanomachines Compete with Nature Biomotors? *ACS Nano* **2009**, 3, 4-9.

15.   Mornet, S.; Vasseur, S.; Grasset, F.; Duguet, E. Magnetic Nanoparticle Design for Medical Diagnosis and Therapy. *J. Mater. Chem.* **2004**, 14, 2161-2175.

16.   Perez, J. M.; Simeone, F. J.; Saeki, Y.; Josephson, L.; Weissleder, R. Viral-Induced Self-Assembly of Magnetic Nanoparticles Allows the Detection of Viral Particles in Biological Media. *J. Am. Chem. Soc.* **2003**, 125, 10192-10193.

17.   Patra, D.; Sengupta, S.; Duan, W.; Zhang, H.; Pavlick, R.; Sen, A. Intelligent, Self-Powered, Drug Delivery Systems. *Nanoscale* **2013**, 5, 1273-1283.

18.   Nair, B. G.; Nagaoka, Y.; Morimoto, H.; Yoshida, Y.; Maekawa, T.; Kumar, D. S. Aptamer Conjugated Magnetic Nanoparticles as Nanosurgeons. *Nanotechnology* **2010**, 21, 455102.

19.   Chwang, A. T.; Wu, T. Y. Hydromechanics of Low-Reynolds-Number Flow. Part 1. Rotation of Axisymmetric Prolate Bodies. *J. Fluid Mech.* **1974**, 63, 607-622.

20.   Silverman, M.; Simon, M. Flagellar Rotation and the Mechanism of Bacterial Motility. *Nature* **1974**, 249, 73-74.

21.   Peyer, K. E.; Zhang, L.; Nelson, B. J. Localized Non-Contact Manipulation Using Artificial Bacterial Flagella. *Appl. Phys. Lett.* **2011**, 99, 174101.

22.   Latham, A. H.; Williams, M. E. Controlling Transport and Chemical Functionality of Magnetic Nanoparticles. *Acc. Chem. Res.* **2008**, 41, 411-420.

23. Chong, W. H.; Chin, L. K.; Tan, R. L. S.; Wang, H.; Liu, A. Q.; Chen, H. Stirring in Suspension: Nanometer‑Sized Magnetic Stir Bars. *Angew. Chem.* **2013**, 125, 8732-8735.

24. Xi, W.; Solovev, A. A.; Ananth, A. N.; Gracias, D. H.; Sanchez, S.; Schmidt, O. G. Rolled-up Magnetic Microdrillers: Towards Remotely Controlled Minimally Invasive Surgery. *Nanoscale* **2013**, 5, 1294-1297.

25. Solovev, A. A.; Xi, W.; Gracias, D. H.; Harazim, S. M.; Deneke, C.; Sanchez, S.; Schmidt, O. G. Self-Propelled Nanotools. *ACS Nano* **2012**, 6, 1751-1756.

26. Goldowsky, J.; Mastrangeli, M.; Jacot-Descombes, L.; Gullo, M. R.; Mermoud, G.; Brugger, J.; Martinoli, A.; Nelson, B.; Knapp, H. F. Acousto-Fluidic System Assisting In-Liquid Self-Assembly of Microcomponents. *J. Micromech. Microeng.* **2013**, 23, 125026.

27. Sinn, I.; Albertson, T.; Kinnunen, P.; Breslauer, D. N.; McNaughton, B. H.; Burns, M. A.; Kopelman, R. Asynchronous Magnetic Bead Rotation Microviscometer for Rapid, Sensitive, and Label-Free Studies of Bacterial Growth and Drug Sensitivity. *Anal. Chem.* **2012**, 84, 5250-5256.

28. Bruus, H. Acoustofluidics 7: The Acoustic Radiation Force on Small Particles. *Lab Chip* **2012**, 12, 1014-1021.

29. Guasto, J. S.; Johnson, K. A.; Gollub, J. P. Oscillatory Flows Induced by Microorganisms Swimming in Two Dimensions. *Phys. Rev. Lett.* **2010**, 105, 168102.

30. Miño, G.; Dunstan, J.; Rousselet, A.; Clément, E.; Soto, R. Induced Diffusion of Tracers in a Bacterial Suspension: Theory and Experiments. *J. Fluid Mech.* **2013**, 729, 423-444.

31. Magdanz, V.; Sanchez, S.; Schmidt, O. G. Development of a Sperm‑Flagella Driven Micro‑Bio‑Robot. *Adv. Mater.* **2013**, 25, 6581-6588.

32. Petit, T.; Zhang, L.; Peyer, K. E.; Kratochvil, B. E.; Nelson, B. J. Selective Trapping and Manipulation of Microscale Objects Using Mobile Microvortices. *Nano Lett.* **2011**, 12, 156-160.

33. Diller, E.; Ye, Z.; Sitti, M. Rotating Magnetic Micro-Robots for Versatile Non-Contact Fluidic Manipulation of Micro-Objects. In *2011 IEEE/RSJ International Conference on Intelligent Robots and Systems*, IEEE: New York, 2011; pp 1291-1296.

34. Happel, J.; Brenner, H. *Low Reynolds Number Hydrodynamics*. Prentice Hall: 1965.

35. Lierke, E. G. Acoustic Levitation - A Comprehensive Survey of Principles and Applications. *Acustica* **1996**, 82, 220-237.

36. Landau, L. D.; Lifshitz, E. M. *Fluid Mechanics*. Pergamon Press: 1987.

37. Liu, L.; Yoo, S. H.; Lee, S. A.; Park, S. Wet-Chemical Synthesis of Palladium Nanosprings. *Nano Lett.* **2011**, 11, 3979-3982.

38. Tottori, S.; Zhang, L.; Qiu, F. M.; Krawczyk, K. K.; Franco-Obregon, A.; Nelson, B. J. Magnetic Helical Micromachines: Fabrication, Controlled Swimming, and Cargo Transport. *Adv. Mater.* **2012**, 24, 811-816.

39. Peyer, K. E.; Tottori, S.; Qiu, F. M.; Zhang, L.; Nelson, B. J. Magnetic Helical Micromachines. *Chem. - Eur. J.* **2013**, 19, 28-38.

40. Li, J.; Sattayasamitsathit, S.; Dong, R.; Gao, W.; Tam, R.; Feng, X.; Ai, S.; Wang, J. Template Electrosynthesis of Tailored-Made Helical Nanoswimmers. *Nanoscale* in press.

41. Xu, J.; Wang, H.; Liu, C.; Yang, Y.; Chen, T.; Wang, Y.; Wang, F.; Liu, X.; Xing, B.; Chen, H. Mechanical Nanosprings: Induced Coiling and Uncoiling of Ultrathin Au Nanowires. *J. Am. Chem. Soc.* **2010**, 132, 11920-11922.

42.   Martin, B. R.; Dermody, D. J.; Reiss, B. D.; Fang, M. M.; Lyon, L. A.; Natan, M. J.;

Mallouk, T. E. Orthogonal Self-Assembly on Colloidal Gold-Platinum Nanorods. *Adv. Mater.*

1999, 11, 1021-1025.

43.   Kestin, J.; Sokolov, M.; Wakeham, W. A. Viscosity of Liquid Water in the Range− 8 C

to 150 C. *J. Phys. Chem. Ref. Data* **1978**, 7, 941-948.

Supporting Information *for* Kilohertz Rotation of Nanorods Propelled by Ultrasound, Traced by Microvortex Advection of Nanoparticles

Andrew L. Balk,[†,‡,△] Lamar O. Mair, [†,‡,△,▽] Pramod P. Mathai, [†,§] Paul N. Patrone, [†,∥,⊥] Wei Wang,[#, □] Suzanne Ahmed,[#] Thomas E. Mallouk,[#] J. Alexander Liddle,[†] and Samuel M. Stavis[†,*]

[†]Center for Nanoscale Science and Technology, National Institute of Standards and Technology, Gaithersburg, Maryland 20899, United States, [‡]Maryland Nanocenter, University of Maryland, College Park, Maryland 20742, United States, [§]Department of Materials Science and Engineering, University of Maryland, College Park, Maryland 20742, United States, [∥]Institute for Research in Electronics and Applied Physics, University of Maryland, College Park, Maryland 20742, United States, [⊥]Institute for Mathematics and its Applications, University of Minnesota, Minneapolis, Minnesota 55455, United States, and [#]Department of Chemistry, The Pennsylvania State University, University Park, Pennsylvania 16802, United States. [△]A. L. Balk and L. O. Mair contributed equally to this research. [▽]Present address: Weinberg Medical Physics LLC, Bethesda, Maryland 20817, United States. [□]Present address: School of Material Science and Engineering, Shenzhen Graduate School, Harbin Institute of Technology, University Town, Shenzhen 518055, China. *Address correspondence to samuel.stavis@nist.gov.

Simplifying Assumptions. We make several simplifying assumptions in our use of a purely hydrodynamic model to describe the interaction between a nanomotor and nanoparticle and infer the rotational frequency of a nanomotor. First, we assume a quasi-static Stokes flow around a nanomotor,

$$\overrightarrow{\nabla p} = \mu\big(\partial_{xx} + \partial_{yy} + \partial_{zz}\big)\vec{v},$$

$$\nabla \cdot \vec{v} = 0,$$

where p is the pressure, $\vec{v}$ is the velocity, and μ is the dynamic viscosity of the fluid. We image the motion of nanomotors and nanoparticles at a frame rate of ≈ 0.3 kHz, which is four orders of magnitude slower than the ultrasonic excitation frequency of ≈ 3 MHz. This temporal coarse graining, as well as the negligible average velocities of the nanomotors and nanoparticles relative to the speed of sound, allow us to treat the flow as incompressible,[1] even though we are considering an explicitly acoustic phenomenon. The minimum distance between the boundaries of the acoustic resonator and nanomotors and nanoparticles of ≈ 100 μm is two orders of magnitude larger than the hydrodynamic radii of these objects of $\approx (150$ to $200)$ nm, so that the flows around these objects are effectively unbounded. From the inferred rotational frequencies of nanomotors of $f_m \approx (0.5$ to $2.5)$ kHz, we estimate a Reynolds number of

$Re < 10^{-3}$ and a viscous penetration depth of $\sqrt{2\nu/\omega_m} > 8$ μm, where ν is the kinematic viscosity and ω_m is the angular speed of a nanomotor, which is significantly larger than our typical radial distances of $R \approx (1 \text{ to } 3)$ μm. Both values are consistent with our assumption of a quasi-static Stokes flow.

Next, we assume that only hydrodynamic forces from a microvortical flow act on a nanoparticle. We input an electrical power $P < 1$ W into our piezoelectric transducer and estimate the time averaged acoustic energy density in one cycle of the incoming acoustic wave as $E = \sigma \left(\frac{P}{f_d}\right)\left(\frac{d}{D}\right)^2\left(\frac{1}{V}\right)$, where σ is the efficiency of the electric to acoustic energy transfer from the piezoelectric transducer to the water, $f_d \approx 3$ MHz is the driving frequency of the piezoelectric transducer, $d = 2$ mm and $D = 12$ mm are the diameters of the resonator and piezoelectric transducer, respectively, and $V = 0.785$ mm^3 is the volume of the fluid in the resonator. We model the energy flux from the surface of the transducer to the surrounding as being uniformly distributed, so that only an energy flux proportional to the area fraction $\left(\frac{d}{D}\right)^2$ is transferred to the water in the resonator. Assuming an efficiency $\sigma = 0.8$, we calculate an acoustic energy density of $E = 9.4$ J $\cdot$ m^{-3} within our resonator. Using this value, we estimate acoustophoretic velocities (see, for example, eq 32 of ref 2) of a polystyrene nanoparticle of $\approx (16 \text{ to } 48)$ nm $\cdot$ s^{-1} towards the planar pressure node, which is also the planar velocity antinode, at radial distances of $R \approx (1 \text{ to } 3)$ μm above and below the nodal plane, at a water temperature of $T = 295$ K. In this estimate, we take the temperature dependence of water viscosity into account, but we assume that the acoustic contrast factor of polystyrene in water at a temperature of $T \approx 295$ K is unchanged from the value of 0.19 at a temperature of $T = 293$ K.[3] This range of estimated acoustophoretic velocities is three orders of magnitude slower than the tangential speeds of $U_\theta \approx (10 \text{ to } 100)$ μm $\cdot$ s^{-1} resulting from the microvortex

advection of a nanoparticle around a nanomotor in the nodal plane. This allows us to ignore any flattening of the circular trajectory of the nanoparticle due to acoustophoresis above and below, but within a few micrometers of, the nodal plane. We note that the acoustophoretic velocities of polystyrene nanoparticles are faster, further above and below the nodal plane. Any acoustic radiation scattered from the nanomotor towards the nanoparticle has an even smaller effect on the velocity of the nanoparticle. Since our experiments occur near the planar pressure node, the secondary radiation interaction is dominated by the compressible motion of the nanomotor and nanoparticle.[4] By considering this secondary interaction between the nanoparticle and a sphere of the same diameter as the nanomotor,[5] we find that the maximum such interaction, in the case that the two objects are in contact, has much less effect on the motion of the nanoparticle than the primary radiative field. Since we have already determined that the effect of the primary radiative field is negligible, the additional fact that the center to center distances between the nanomotor and nanoparticle in our experiments are several times the related diameters leads us to ignore any secondary interaction due to scattered acoustic fields. In addition, as we consider radial distances of $R > 1$ μm, any electrostatic interactions between nanomotors and nanoparticles are mostly screened by mobile ions in deionized water with a resistivity of < 18 MΩ · cm and a Debye length $\lambda_D < 1$ μm.[6]

Finally, we assume that nanomotors and nanoparticles are perfectly rodlike and spherical in shape, respectively. This idealization neglects structural asymmetries of the nanorod ends, such as concavity, that have been previously implicated in the propulsion mechanism associated with nanomotor translation.[7, 8] However, for our nominal distributions of nanorod length and diameter, the observed variations in nanorod end shape have small effects on the hydrodynamic interactions, and thus introduce small errors, in the far field measurements that we make.[9]

Perturbation Estimates. We use two far field analyses, both based on a single iteration of the method of reflections,[9] to estimate a range of values for the hydrodynamic perturbation from the wake of a nanoparticle to the rotational frequency of a nanomotor

$$\delta_f = \left| \frac{f_0 - f_{pert}}{f_0} \right|,$$

where f_{pert} and f_0 are, respectively, the perturbed and unperturbed nanomotor rotational frequencies. In the subsequent analyses, $\vec{r}$ is the vector separating the centers of mass of the nanoparticle and the nanomotor, and we set $z = 0$ in eq 1 of the manuscript[10] to obtain the maximum perturbation condition at a flow speed $U_\theta \approx \frac{\omega_m a b^2}{R\sqrt{a^2 + R^2}}$, where $2a$ and $2b$ are the measured length and diameter of the nanomotor, respectively. We ignore the contribution from the $V_m \approx 10 \ \mu m \cdot s^{-1}$ translation of the nanomotor. A simple calculation shows that this imparts a speed of $\approx 1 \ \mu m \cdot s^{-1}$ to the nanoparticle at $|\vec{r}| \approx 1 \ \mu m$, which is small compared to the measured tangential speeds of $U_\theta \approx (10 \text{ to } 100) \ \mu m \cdot s^{-1}$ due to microvortex advection. Since we do not know if the rotational actuation mechanism provides a constant angular speed or a constant torque, we assume the more conservative case of constant torque. We therefore surmise an unperturbed flow field from the nanoparticle $\vec{v}^{(0)} = U_\theta \approx \frac{\omega_m a b^2}{R\sqrt{a^2 + R^2}}$ and compute the first order correction to this flow field $\vec{v}^{(1)}$. We postulate that the maximum perturbation is less than the absolute value of the ratio of these flow fields evaluated at the nanomotor surface

$$\delta_f = \left| \frac{f_0 - f_{pert}}{f_0} \right| \lesssim \left| \frac{\vec{v}^{(1)}}{\vec{v}^{(0)}} \right| \Bigg|_{R=b}.$$

In our first analysis, we deliberately overestimate the perturbation by artificially imposing an external force to hold a nanoparticle stationary in the microvortical flow field, and we calculate the effect of the additional Stokes drag on the rotation of the nanomotor. In a shift of reference frame, we equivalently determine the perturbation to a stationary flow field of a

nanoparticle translating at a velocity $\vec{u}_t = U_\theta \hat{\jmath}$ and rotating at an angular velocity $\vec{\omega}_t = -\frac{U_\theta}{2}\left(\frac{1}{R} + \frac{R}{a^2+R^2}\right)\hat{k}$, where $\hat{\jmath}$ is the unit vector parallel to the instantaneous velocity of the nanoparticle and $\hat{k}$ is the unit vector parallel to the long axis of the nanomotor. Imposing the boundary conditions on the fluid velocity $\vec{v}$ of

$$\vec{v} \to 0 \qquad as \quad |\vec{r}| \to \infty,$$

$$\vec{v} = \vec{u}_t + \vec{\omega}_t \times \vec{r} \qquad at \quad |\vec{r}| = c,$$

we calculate the additive influence $\vec{v}^{(1)}$ of the nanoparticle on the flow field as

$$\vec{v}^{(1)} = \frac{3}{4}\left(\frac{c}{R} + \frac{c^3}{3R^3}\right)\vec{u}_t + \frac{3}{4}(\vec{u}_t \cdot \vec{r})\left(\frac{c}{R^3} - \frac{c^3}{R^5}\right)\vec{r} + \left(\frac{c^3}{R^3}\right)\vec{\omega}_t \times \vec{r}.$$

Taking the translational and angular velocities stated above and using one iteration of the method of reflections, we calculate the maximum perturbation from a stationary nanoparticle[1] at the surface of the nanomotor, where $\left|\vec{v}^{(0)}\right| = \omega_m b$, as

$$\delta_{f\,(stat)} = \frac{ab}{R\sqrt{a^2+R^2}}\left[\underbrace{\frac{3}{4}\left(\frac{c}{(R-b)} + \frac{c^3}{3(R-b)^3}\right)}_{Translation} + \underbrace{\frac{c^3}{2(R-b)^2}\left(\frac{1}{R} + \frac{R}{a^2+R^2}\right)}_{Rotation}\right].$$

In our second analysis, we consider that, in the absence of net forces and torques, the quasi–steady Stokes flow will advect an ideal tracer with the same velocity as the average flow field at the tracer location. Assuming that the nanoparticle and nanomotor are far apart, we linearize the flow field near the nanoparticle

$$\vec{v}^{(0)}(\vec{r} + \Delta\vec{r}) \approx \vec{v}^{(0)}(\vec{r}) + \nabla\vec{v}^{(0)}\big|_{\vec{r}}\Delta\vec{r},$$

where

$$\nabla\vec{v}^{(0)} = \begin{bmatrix} \partial_x v_x & \partial_y v_x & \partial_z v_x \\ \partial_x v_y & \partial_y v_y & \partial_z v_y \\ \partial_x v_z & \partial_y v_z & \partial_z v_z \end{bmatrix}.$$

Using eq 1 from the manuscript, we can then show that the only non-zero terms of $\nabla\vec{v}^{(0)}\big|_{\vec{r}}$ are the two off diagonal elements $\partial_x v_y$ and $\partial_y v_x$, corresponding to the fact the flow field changes

direction away from the nanoparticle, and the speed of the flow decreases as we move further from the nanomotor. Assuming that the net torque on the nanoparticle is zero, this causes the nanoparticle to rotate about the z–axis. Additionally, we note that perturbations from these terms, when linearly combined, partially cancel. This allows us to only compute the effect of the larger term, $\partial_y v_x$, which will determine the asymptotic nature of the perturbation. Thus we can solve the Stokes equations subject to the boundary conditions on the fluid velocity $\vec{v}$ of

$$\vec{v}^{(1)} \to 0 \qquad\qquad as \quad |\vec{r}| \to \infty,$$

$$v_x^{(0)} + v_x^{(1)} \approx v_x^{(0)}\big|_{\vec{r}} + y\gamma + v_x^{(1)} = -\omega y \qquad at \quad |\vec{r}| = c,$$

$$v_y^{(0)} + v_y^{(1)} \approx v_y^{(1)} = \omega x \qquad at \quad |\vec{r}| = c,$$

$$v_z^{(0)} + v_z^{(1)} = v_z^{(1)} = 0 \qquad at \quad |\vec{r}| = c,$$

where the shear rate $\gamma = \partial_y v_x$. Assuming that the nanoparticle follows the streamlines of the local flow based on the zero net force assumption, we solve[11] for $\vec{v}^{(1)}$, changing from vector $\vec{r}$ to scalar R

$$v_x^{(1)}{}_{(x,y,z)} = \frac{-\omega y c^3}{R^3} + \omega c^3 \left[\frac{y}{R^3} + \frac{5x^2 y}{R^5}\right] + \omega c^5 \left[\frac{y}{R^5} - \frac{5x^2 y}{R^7}\right],$$

$$v_y^{(1)}{}_{(x,y,z)} = \frac{\omega x c^3}{R^3} - \omega c^3 \left[\frac{x}{R^3} - \frac{5xy^2}{R^5}\right] + \omega c^5 \left[\frac{x}{R^5} - \frac{5xy^2}{R^7}\right],$$

$$v_z^{(1)}{}_{(x,y,z)} = \frac{5\omega c^3 xyz}{R^5}\left(1 - \frac{c^2}{R^2}\right),$$

$$p^{(1)}{}_{(x,y,z)} = \frac{10\mu\omega c^3 xy}{R^5}.$$

By assuming that the net torque on the nanoparticle is zero, one can show that the solution to these equations[11] gives the perturbation as

$$\delta_{f\,(trac)} \le \underbrace{\frac{ab^2}{R\sqrt{a^2+R^2}}\left[\frac{1}{R} + \frac{R}{a^2+R^2}\right]\left[\frac{5c^3}{2b(R-b)^2} + \frac{3c^5}{b(R-b)^4}\right]}_{Rotation}.$$

Our two estimated perturbations, $\delta_{f_{(stat)}}$ and $\delta_{f_{(trac)}}$, are plotted as a function of R for a nanoparticle of hydrodynamic radius $c = 200$ nm in Figure S1. The perturbation from a stationary nanoparticle is shown in red, the perturbation from a freely advecting tracer is shown in blue, and the minimum radius of microvortex advection events that we quantitatively analyze is shown in gray. For a tracer, the perturbation is $\delta_f < 0.5\,\%$ for $R > 1$ µm, which is negligibly small compared to the other sources of uncertainty in our measurements. Therefore, the nanoparticles qualify as effectively noninteracting tracers of microvortical flows in our experimental study.
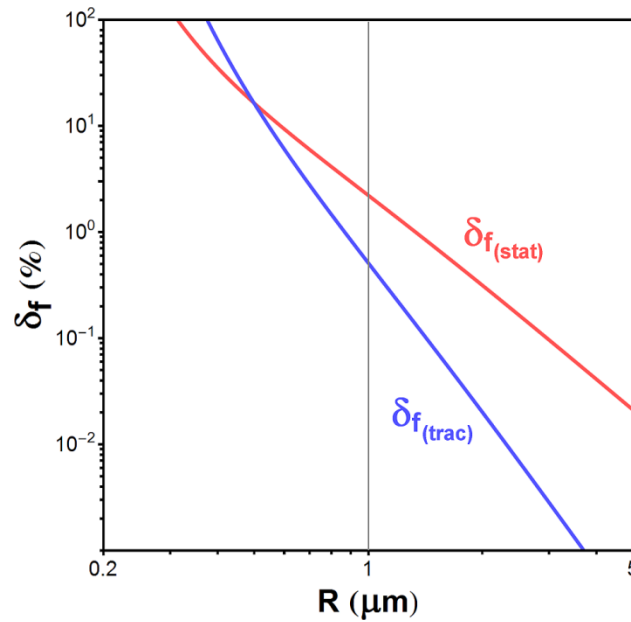

Figure S1. Nanoparticles of hydrodynamic radius $c \approx 200\,nm$ qualify as effectively noninteracting tracers of microvortical fluid flow at interaction radii of $R > 1$ µm. The perturbation from the wake of a stationary nanoparticle to the rotation of a nanomotor is shown in red, the perturbation from the wake of a freely advecting tracer is shown in blue, and the minimum interaction radius of the microvortex advection events that we analyze quantitatively is shown in gray. For a freely advecting tracer, the hydrodynamic perturbation is $\delta_f < 0.5\,\%$ for $R > 1$ µm, which is negligibly small compared to other sources of uncertainty in our measurements.

Image Analysis. Our image analysis algorithm localizes a nanomotor and a nanoparticle in four stages, as shown in Figure S2. Nanomotors and nanoparticles are first localized within each frame of a video. The nanomotor is identified as the largest and brightest feature in each video frame, and the centroid of this feature is set as the center of a region of interest (ROI), as shown in Figure S2a. This ROI is fitted to an analytical model composed of four spatially offset error functions, describing the image of a nanorod with edges blurred by optical diffraction, as shown in Figure S2b. The nanorod length and diameter are fixed while the nanorod position, orientation, and intensity are floated as adjustable parameters, so that this fit is insensitive to the presence of the nanoparticle. This fit is subsequently subtracted from the ROI, leaving a residual ROI containing only the nanoparticle, as shown in Figure S2c. The nanoparticle is identified as the brightest feature in the residual ROI, assuming that the nanoparticle is not obscured by the nanomotor. The residual ROI is fitted to a radially symmetrical Gaussian function with a fixed variance, describing the image of a sphere with a diameter that is near to the optical diffraction limit. The nanoparticle position is then transformed into the reference frame of the nanomotor.
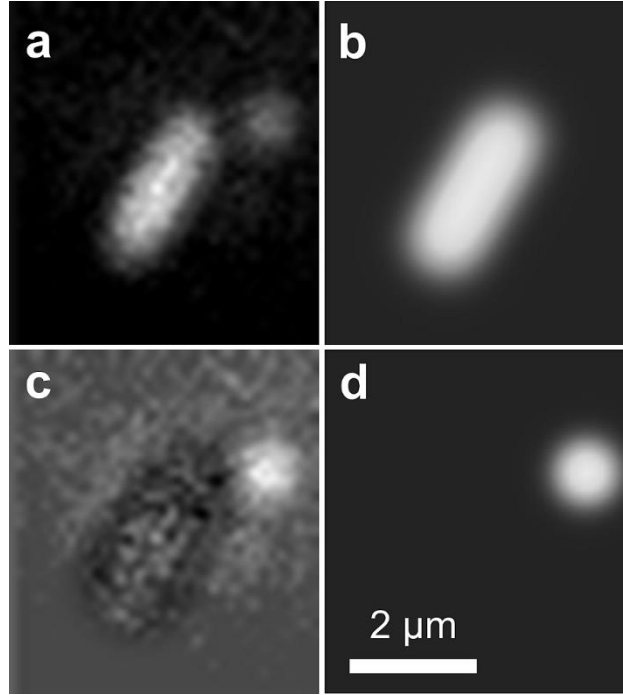
Figure S2. Our image analysis algorithm localizes and orients a nanomotor and a nanoparticle in four stages. (a) A video frame is spatially and temporally cropped into a region of interest (ROI) around the nanomotor centroid. (b) The nanomotor, as the brightest and largest feature in the ROI, is fit to four error functions to localize and orient the nanomotor. (c) The residual of this fit leaves only the nanoparticle in a residual ROI. (d) The brightest feature in the residual ROI is fit to a two dimensional radially symmetric Gaussian function.

Tracking Analysis. Our tracking algorithm follows the motion of nanoparticles and nanomotors between multiple frames of a video. The nanomotor position as a function of time data is fit to a linear function to extract the average speed of the nanomotor V_m (not shown). To extract average values of U_θ and R during microvortex advection, the projected images of a tracer nanoparticle moving in a circular trajectory around a nanomotor are analyzed, assuming that U_θ and R are constant during each microvortex advection event of $\geq \pi$ radians, giving a constant angular speed $\phi_t = U_\theta R < \omega_m$, as illustrated in Figure S3a. This analytical model is reasonable considering our experimental values of Brenner number $Br \gtrsim 10$, as well as the

negligible acoustophoretic flattening of the nanoparticle trajectory around the planar velocity antinode. The projected center to center distance ρ between a nanomotor and a nanoparticle as a function of time is fitted to a sinusoidal function $\rho = R \cdot sin[\phi_t t]$. From this fit, values of U_θ and R are extracted, averaging over variation in these two values due to stochastic diffusion. Simulated data depicting ρ as a function of time for three microvortex advection events occurring at different values of U_θ and R is shown in Figure S3b. The simulated data is undefined within a range of -0.8 μm $\lesssim \rho \lesssim 0.8$ μm as the nanomotor obscures the tracer.
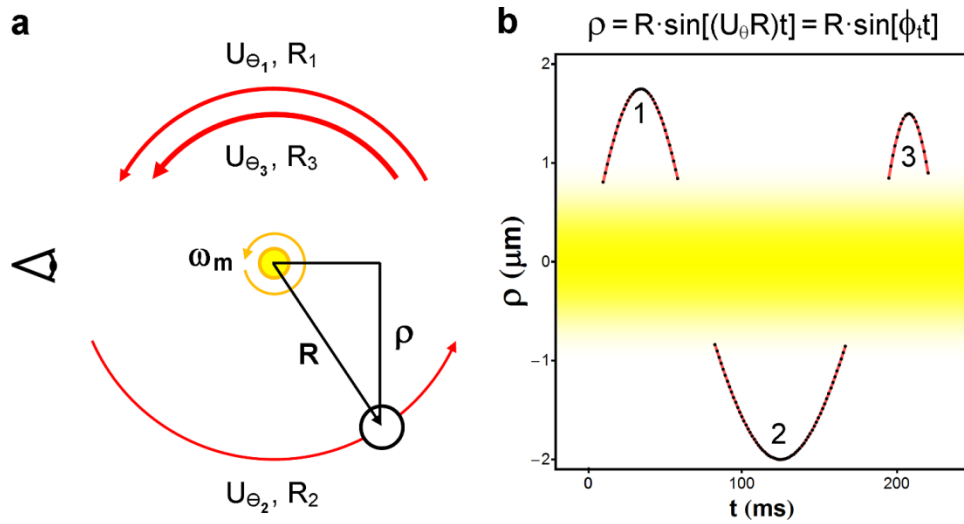

Figure S3. We measure U_θ and R by fitting the two dimensional projection of three dimensional circular motion due to microvortex advection to a sinusoidal function. (a) A schematic, approximately to scale, shows a tracer advecting around a nanomotor at three different values of angular speed $\phi_t = U_\theta R < \omega_m$. Thicker red lines denote larger values of U_θ. An observer at the left sees the projected radial distance ρ. (b) Simulated data shows $\rho(t)$ for the three microvortex advection events. The data is undefined for -0.8 μm $\lesssim \rho \lesssim 0.8$ μm as the nanomotor obscures the tracer.

Variation and Uncertainty in Inferred Values of Rotational Frequency

	Rotational Frequency f_m (kHz)	Standard Uncertainty (kHz)
Nanomotor shown in Figure 4c		
Microvortex Advection 1	1.34	0.47
Microvortex Advection 2	0.91	0.24
Microvortex Advection 3	0.70	0.20
Microvortex Advection 4	0.93	0.24
Microvortex Advection 5	1.30	0.35
Microvortex Advection 6	1.31	0.38
Average ± Standard Deviation	1.08 ± 0.25	0.31 ± 0.09
Nanomotor shown in Figure 4d		
Microvortex Advection 1	1.33	0.42
Microvortex Advection 2	1.25	0.34
Microvortex Advection 3	2.41	0.87
Microvortex Advection 4	0.75	0.24
Microvortex Advection 5	1.34	0.41
Microvortex Advection 6	1.83	0.66
Average ± Standard Deviation	1.49 ± 0.52	0.49 ± 0.21

Table S1. A comparison of the persistent microvortex advection of tracer nanoparticles around two nanomotors shows variation and uncertainty in inferred values of rotational frequency f_m.

Video S1. A nanoparticle advects in a microvortex around a rotating nanorod while a less proximal nanoparticle diffuses. The video has been contrast enhanced and reflected about the vertical axis for clarity of presentation. The video frame dimensions are 10.35 μm wide by 9.43 μm high.

Video S2. A nanoparticle advects in a microvortex around a rotating nanorod for $\approx 8\pi$ radians. The video has been contrast enhanced and reflected about the vertical axis for clarity of presentation. The video frame dimensions are 11.00 μm wide by 9.83 μm high.

REFERENCES AND NOTES

1.   Landau, L. D.; Lifshitz, E. M. *Fluid Mechanics*; Pergamon Press: Oxford, 1987.

2.   Bruus, H. Acoustofluidics 7: The Acoustic Radiation Force on Small Particles. *Lab Chip* **2012**, 12, 1014-1021.

3.   Weast, R. C.; Astle, M. J.; Beyer, W. H. *CRC Handbook of Chemistry and Physics*; CRC Press: Boca Raton: 1988.

4.   Groschl, M. Ultrasonic Separation of Suspended Particles - Part I: Fundamentals. *Acustica* **1998**, 84, 432-447.

5.   Haake, A. *Micromanipulation of Small Particles with Ultrasound* PhD Thesis of the Swiss Federal Institute of Technology Zurich, Switzerland, 2001.

6.   Israelachvili, J. N. *Intermolecular and Surface Forces (With Applications to Colloidal and Biological Systems)*; Academic Press: London, 1985.

7.   Ahmed, S.; Wang, W.; Mair, L. O.; Fraleigh, R. D.; Li, S.; Castro, L. A.; Hoyos, M.; Huang, T.; Mallouk, T. E. Steering Acoustically Propelled Nanowire Motors Towards Cells in a Biologically Compatible Environment Using Magnetic Fields. *Langmuir* **2013**, 29, 16113-16118.

8.   Garcia-Gradilla, V.; Orozco, J.; Sattayasamitsathit, S.; Soto, F.; Kuralay, F.; Pourazary, A.; Katzenberg, A.; Gao, W.; Shen, Y. F.; Wang, J. Functionalized Ultrasound-Propelled Magnetically Guided Nanomotors: Toward Practical Biomedical Applications. *ACS Nano* **2013**, 7, 9232-9240.

9.   Happel, J.; Brenner, H. *Low Reynolds Number Hydrodynamics*; Prentice Hall: New Jersey, 1965.

10.   Chwang, A. T.; Wu, T. Y. Hydromechanics of Low-Reynolds-Number Flow. Part 1. Rotation of Axisymmetric Prolate Bodies. *J. Fluid Mech.* **1974**, 63, 607-622.

11.   Pozrikidis, C. *Introduction to Theoretical and Computational Fluid Dynamics*; Oxford University Press: New York, 1997.